

Extended energy range analysis for angle-resolved time-of-flight photoelectron spectroscopy ^{EP}

Cite as: J. Appl. Phys. **124**, 164504 (2018); <https://doi.org/10.1063/1.5048515>

Submitted: 15 July 2018 . Accepted: 05 October 2018 . Published Online: 23 October 2018

 Michael Huth,  Andreas Trützschler,  Cheng-Tien Chiang,  Robin Kamrta, Frank O. Schumann,  Wolf Widdra, et al.

COLLECTIONS

 This paper was selected as an Editor's Pick



View Online



Export Citation



CrossMark

ARTICLES YOU MAY BE INTERESTED IN

[SiO₂/Si\(001\) studied by time-resolved valence band photoemission at MHz repetition rates: Linear and nonlinear excitation of surface photovoltage](#)

Journal of Vacuum Science & Technology A **37**, 021101 (2019); <https://doi.org/10.1116/1.5082188>

[Time- and momentum-resolved photoemission studies using time-of-flight momentum microscopy at a free-electron laser](#)

Review of Scientific Instruments **91**, 013109 (2020); <https://doi.org/10.1063/1.5118777>

[Electron pair emission detected by time-of-flight spectrometers: Recent progress](#)

Applied Physics Letters **104**, 061602 (2014); <https://doi.org/10.1063/1.4864274>

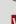
HIDEN
ANALYTICAL

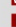
Instruments for **Advanced Science**

- Knowledge,
- Experience,
- Expertise

[Click to view our product catalogue](#)

Contact Hiden Analytical for further details:

 www.HidenAnalytical.com

 info@hiden.co.uk



Gas Analysis

- ▶ dynamic measurement of reaction gas streams
- ▶ catalysis and thermal analysis
- ▶ molecular beam studies
- ▶ dissolved species probes
- ▶ fermentation, environmental and ecological studies



Surface Science

- ▶ UHVTPD
- ▶ SIMS
- ▶ end point detection in ion beam etch
- ▶ elemental imaging - surface mapping



Plasma Diagnostics

- ▶ plasma source characterization
- ▶ etch and deposition process reaction kinetic studies
- ▶ analysis of neutral and radical species



Vacuum Analysis

- ▶ partial pressure measurement and control of process gases
- ▶ reactive sputter process control
- ▶ vacuum diagnostics
- ▶ vacuum coating process monitoring



Extended energy range analysis for angle-resolved time-of-flight photoelectron spectroscopy

Michael Huth,¹ Andreas Trützscher,^{1,2} Cheng-Tien Chiang,^{1,2,a)} Robin Kamrla,^{1,2} Frank O. Schumann,^{1,b)} and Wolf Widdra^{1,2,c)}

¹Max Planck Institute of Microstructure Physics, Weinberg 2, D-06120 Halle (Saale), Germany

²Institute of Physics, Martin-Luther-Universität Halle-Wittenberg, Von-Danckelmann-Platz 3, D-06120 Halle (Saale), Germany

(Received 15 July 2018; accepted 5 October 2018; published online 23 October 2018)

An approximation method for electrostatic time-of-flight (ToF) spectroscopy on photoelectrons distributed over a wide energy range is presented. This method is an extension of conventional analysis and aims at specific energy and angular regions, where distinctly different emission angles and energies are mapped to the same ToF and detector position by the spectrometer. The general formulation and the systematic errors are presented, and a practical example is demonstrated for photoelectrons from Ag(001) with kinetic energies of 0.5–25 eV. © 2018 Author(s). All article content, except where otherwise noted, is licensed under a Creative Commons Attribution (CC BY) license (<http://creativecommons.org/licenses/by/4.0/>). <https://doi.org/10.1063/1.5048515>

I. INTRODUCTION

Time-of-flight (ToF) spectroscopy of charged particles allows the detection of many spectroscopic channels in parallel. In ion mass spectroscopy, a wide range of charge to mass ratio of ions is analyzed simultaneously,^{1,2} and in electron spectroscopy, a large phase space of emission angle and kinetic energy can be acquired at the same time using angle-resolving detection.^{3,4} Recently, due to the importance of angle-resolved photoelectron spectroscopy (ARPES) on studying electronic properties of novel materials, ToF spectroscopy of photoelectrons has been developed remarkably.^{5–12}

In contrast to conventional hemispherical energy analyzers, in ToF-based ARPES, the two-dimensional (2D) emission angular distribution (θ , ϕ) and the corresponding energy (E) spectra are measured in a single experiment.^{3,4} Generally, a ToF spectrometer acquires the hit position of an individual photoelectron (x , y) on a 2D detector and its ToF from the sample to the detector (t). In an ideal case, the spectrometer should perform a one-to-one mapping from $(\theta$, ϕ , E) to $(x$, y , t), which allows $(\theta$, ϕ , E) to be retrieved from the detected $(x$, y , t) coordinates as shown in Fig. 1(a).

However, the one-to-one forward mapping can only be guaranteed in a limited energy and angular range,^{13,14} beyond which the ToF spectrometer performs a many-to-one forward mapping from $(\theta$, ϕ , E) to $(x$, y , t) such as in Fig. 1(b). The restricted energy range of the one-to-one mapping not only puts an upper bound for the efficiency of ToF spectroscopy but may also inhibit advanced experiments, where a wide energy range is especially desirable. An example for such experiments is coincidence photoelectron

spectroscopy,^{15–19} where the total detection efficiency scales quadratically with that of the individual spectrometer.²⁰

In this paper, we present a general extension of the conventional method to analyze the photoelectron events in a ToF-based spectrometer. This analysis includes the many-to-one forward mapping such as in Fig. 1(b) and allows one to extend the available angular and energy range. The method is based on assumptions for the distribution among the multiple (θ_i, ϕ_i, E_i) events that are mapped to the same (x, y, t) detector coordinates by the ToF spectrometer. The resultant systematic error in the retrieved emission coordinates of photoelectrons (θ, ϕ, E) can be quantified according to the imaging properties of the spectrometer. In the following, we describe this approximation and illustrate it with a commercial ToF spectrometer.²¹ As an example, we apply this analysis to ARPES on a Ag(001) with photoelectrons distributed over a kinetic energy range from 0.5 to 25 eV.

II. FORMULATION OF APPROXIMATION

In conventional analyses, the one-to-one mapping in Fig. 1(a) is considered as a transformation between an infinitesimal volume $\Delta x \times \Delta y \times \Delta t$ around the detector coordinates (x, y, t) to a volume element $\Delta\theta \times \Delta\phi \times \Delta E$ in the photoemission configuration space (θ, ϕ, E) . The analyses rely on a grid in the (x, y, t) space consisting of contours with constant θ , ϕ , and E , which are calculated beforehand by simulations of electron trajectories. For each individual photoelectron, the event detected with its (x, y, t) coordinates, an interpolation between the contours of the grid is performed in order to obtain the corresponding (θ, ϕ, E) values. The work flow of the conventional analysis is shown by the left side of Fig. 2 (black), and its precision can be estimated from experiments, where the resolutions of the spectrometers are examined in detail. Typical values of optimal resolutions can be better than 0.2° and 5 meV with spectrometer settings of low kinetic (E_{kin}) and pass energies (E_{pass}).^{4,11} These

^{a)}Electronic mail: cheng-tien.chiang@physik.uni-halle.de

^{b)}Electronic mail: schumann@mpi-halle.de

^{c)}Electronic mail: wolf.widdra@physik.uni-halle.de



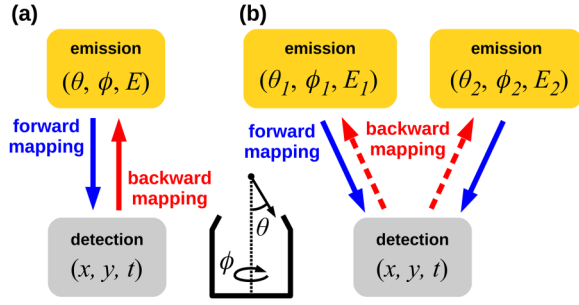


FIG. 1. (a) One-to-one mapping from the photoelectron emission angles (θ, ϕ) and kinetic energy (E) to the hit position on the 2D detector (x, y) and ToF (t) . For small regions in the θ - ϕ - E configuration space, multiple θ - ϕ - E combinations lead to identical detection events as illustrated by the two-to-one mapping from (θ, ϕ, E) to (x, y, t) in (b). The approximated backward mapping is indicated by the dashed arrows. The inset exemplifies the polar (θ) and the azimuthal (ϕ) angles with respect to the spectrometer axis (dotted) in the case of a cylindrical ToF spectrometer.

settings are specifically chosen for high energy resolution whereas the available energy window is only of few eV wide. For wide energy applications, settings with a higher E_{pass} need to be applied, resulting in an inevitable trade-off to a lower energy resolution. In this paper, we will demonstrate an application of wide energy range, which will have an energy resolution of about 180 meV in the conventional analysis²² and will be discussed in detail later.

Whereas conventional analyses do not introduce additional uncertainties formally, in practice their accuracies are limited by the precision of the electron trajectory simulations as well as the spatial and time resolutions of the

detector. For example, considering two individual events which are detected in proximity much closer than the spatial and time resolutions of the detector, their detector coordinates (x, y, t) cannot be distinguished from each other despite of their distinctly different emission coordinates (θ, ϕ, E) . As a result, these two events are *apparently* related to the same detector coordinates due to the limited detector resolutions, as if they would be mapped by the spectrometer in a two-to-one forward mapping as in Fig. 1(b). Therefore, in spite of the formally well-defined boundary between the one-to-one and the many-to-one mappings as shown in Fig. 1, in practical analyses, this boundary is determined by the detector resolutions and the precision of the trajectory simulations.

For cases where the different (θ, ϕ, E) coordinates in a many-to-one mapping have only small discrepancies as compared to the spectrometer resolution, they can be evaluated without a significant degradation of the overall resolution. To perform such an evaluation, an assumption regarding the distribution among the different (θ, ϕ, E) coordinates in the many-to-one mapping is required. For clarity, we illustrate our approximation for the backward mapping of the two-to-one mapping in Fig. 1(b) as follows:

With weighting w_1 :

$$\Delta x \times \Delta y \times \Delta t \rightarrow \Delta\theta_1 \times \Delta\phi_1 \times \Delta E_1$$

$$(x, y, t) \rightarrow (\theta_1, \phi_1, E_1).$$

With weighting w_2 :

$$\Delta x \times \Delta y \times \Delta t \rightarrow \Delta\theta_2 \times \Delta\phi_2 \times \Delta E_2$$

$$(x, y, t) \rightarrow (\theta_2, \phi_2, E_2).$$

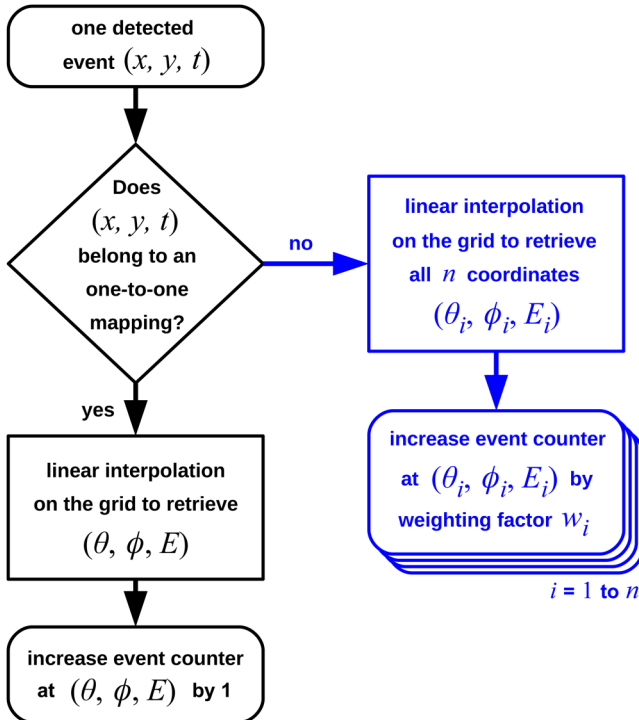


FIG. 2. Work flow of conventional analysis for one-to-one mapping (black) and the approximated method to analyze the many-to-one mapping (blue). Detected photoelectrons are registered in the photoelectron spectrum by the event counter.

In this approximation, we assign the detected event at (x, y, t) with a weighting factor w_1 to the emission coordinates (θ_1, ϕ_1, E_1) , and with a factor w_2 to (θ_2, ϕ_2, E_2) . Assumptions of factors w_1 and w_2 need to be made, which should not generate features only at some specific energy or angular coordinates. Moreover, these factors need to be normalized by $w_1 + w_2 = 1$ since the number of events should be conserved in both the forward and the backward mappings. In a general case of an n -to-one forward mapping, where n different (θ_i, ϕ_i, E_i) with $i = 1$ to n are mapped to the same (x, y, t) , n different weighting factors are needed with a constraint $\sum_{i=1}^n w_i = 1$. In Fig. 2, this work flow for the many-to-one mapping is shown (blue).

The systematic error due to this approximation can be quantified by considering an incident photoelectron with emission coordinates $(\theta_{in}, \phi_{in}, E_{in})$ that arrives in the spectrometer at the detector coordinates (x, y, t) . In case (x, y, t) do not allow a one-to-one backward mapping, this event must stem from n different emission coordinates with $n > 1$. The approximated backward mapping will deliver these n different emission coordinates (θ_i, ϕ_i, E_i) , each with a corresponding weighting factor w_i . Since only one set of the n different (θ_i, ϕ_i, E_i) coordinates matches $(\theta_{in}, \phi_{in}, E_{in})$, the difference between $(\theta_{in}, \phi_{in}, E_{in})$ and the other $n-1$ sets of (θ_i, ϕ_i, E_i) leads to errors in the approximated backward

mapping. The resultant systematic error in energy and emission angles due to the approximated backward mapping can be evaluated as

$$\sigma_E = \sqrt{\sum_{i=1}^n w_i \times (E_i - E_{in})^2},$$

$$\sigma_\theta = \sqrt{\sum_{i=1}^n w_i \times (\theta_i - \theta_{in})^2}. \quad (1)$$

Similarly, the systematic error for the emission angle ϕ can be calculated. These errors have an upper bound as given by the maximum difference between the n different values of (θ_i, ϕ_i, E_i) . Take σ_E for the case of $n = 2$ as an example, its upper bound is $\sigma_E^{max} = E^{max} - E^{min}$ according to Eq. (1),²³ where E^{max} and E^{min} are the maximum and the minimum, respectively, among the two different values of E_i . Generally, the errors σ_E , σ_θ , and σ_ϕ depend on w_i . Often the possible photoemission events that are mapped to the same (x, y, t) are rather close to each other in the (θ_i, ϕ_i, E_i) configuration space, and the formal ambiguity might introduce only a small error.

III. PRACTICAL EXAMPLE

In the following, we demonstrate a practical example for the approximated backward mapping in Sec. II using a commercial ToF spectrometer.^{11,21} The settings of the spectrometer are wide-angle-mode with a nominal kinetic energy (E_{kin}) of 8 eV and a pass energy (E_{pass}) of 60 eV. Due to the cylindrical symmetry with respect to the optical axis of the spectrometer, the three-dimensional (3D) emission coordinates (θ, ϕ, E) can be reduced to (θ, E) and displayed on the 2D plane as shown in Fig. 3(a). Correspondingly, the 3D volume $\Delta\theta \times \Delta\phi \times \Delta E$ is reduced to an area of a triangle $\Delta\theta \times \Delta E/2$. Here, we intentionally use a triangular grid

instead of a rectangular grid, since only a triangle can be mapped to the detector space in general without producing any additional crossing between its edges. As shown in Fig. 3(a), the triangles are defined by neighboring (θ, E) points and cover the spectrometer acceptance range. In Fig. 3(a), a low resolution of $\Delta\theta$ and ΔE is selected for better visualization.

The emission coordinates (θ, E) are connected to the detector coordinates (r, t) by the forward mapping according to the electrostatic model of the spectrometer.²⁴ Here, the radial position r appears instead of the 2D coordinates (x, y) due to the cylindrical symmetry, and its origin is located at the spectrometer axis.²⁵ As a consequence, the forward mapping transforms the (θ, E) grid in Fig. 3(a) to the (r, t) grid in Fig. 3(b).

A. Two-to-one forward mapping

To illustrate a practical example of the two-to-one forward mapping as formally outlined in Fig. 1(b), we consider two triangular elements on the (θ, E) plane in Fig. 3(a) (filled) and their corresponding triangles on the (r, t) plane in Fig. 3(b). As shown in the insets of Fig. 3(b), these two triangles have an overlap on the (r, t) plane. As a consequence, detected events in this overlapping (r, t) region can originate from either of the two triangles on the (θ, E) plane. As an example, two independent events with different emission angles and energies are indicated by the blue dots in the inset of Fig. 3(a), which arrive at the same detector coordinates as indicated in the inset of Fig. 3(b). Consequently, a two-to-one forward mapping occurs within this overlapping (r, t) region and it corresponds to the formal situation in Fig. 1(b).

B. Error estimation

The error estimation in the approximated backward mapping is a crucial aspect to judge the usefulness of the

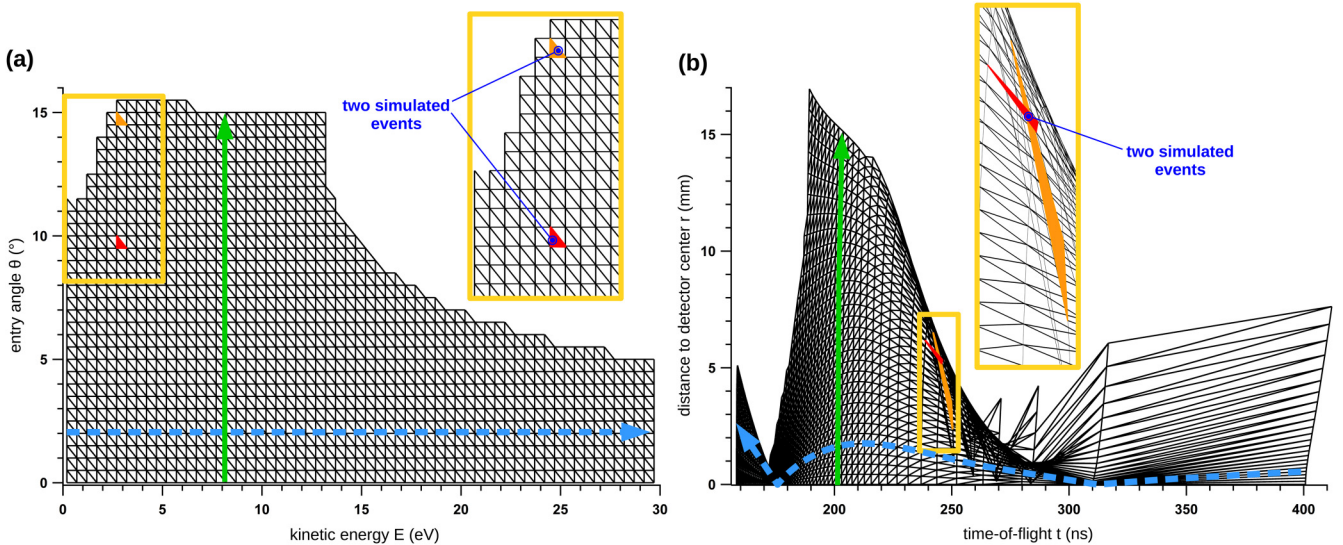


FIG. 3. (a) Grid of the (θ, E) emission coordinates of photoelectrons entering the ToF-spectrometer²¹ and (b) the corresponding grid of the (r, t) detector coordinates after the forward mapping. The insets (yellow boxes) show two simulated events (blue dots) with different (θ, E) arriving at the same (r, t) . Such a two-to-one forward mapping is indicated by the overlapping region between the filled triangles (colored) in (b). Solid and dashed arrows indicate exemplary contours with a constant E and a constant θ , respectively.

extended analysis. Ideally, the backward mapping should transform the detector coordinates (r, t) in Fig. 3(b) to the emission coordinates (θ, E) in Fig. 3(a) without introducing any error. However, since in the forward mapping an n -to-one mapping with $n > 1$ can occur as shown in Fig. 1(b) and described in Sec. III A, the approximated backward mapping as formulated in Sec. II is required. In Fig. 4(a), the order n for the spectrometer settings in Fig. 3 is shown. Note that in a practical application, mainly regions with $n \leq 3$ will be used. In the approximated backward mapping, we assume a distribution of the weighting factor w_i proportional to the solid angle Ω_i in the proximity of the (θ_i, E_i) emission coordinates and inversely proportional to its corresponding area A_i on the (r, t) plane,

$$w_i = \frac{\Omega_i/A_i}{\sum_{i=1}^n \Omega_i/A_i}. \quad (2)$$

Here, the normalization condition $\sum_{i=1}^n w_i = 1$ is fulfilled by the summation in the denominator. With this choice of w_i , the original distribution of photoelectrons can be retrieved if

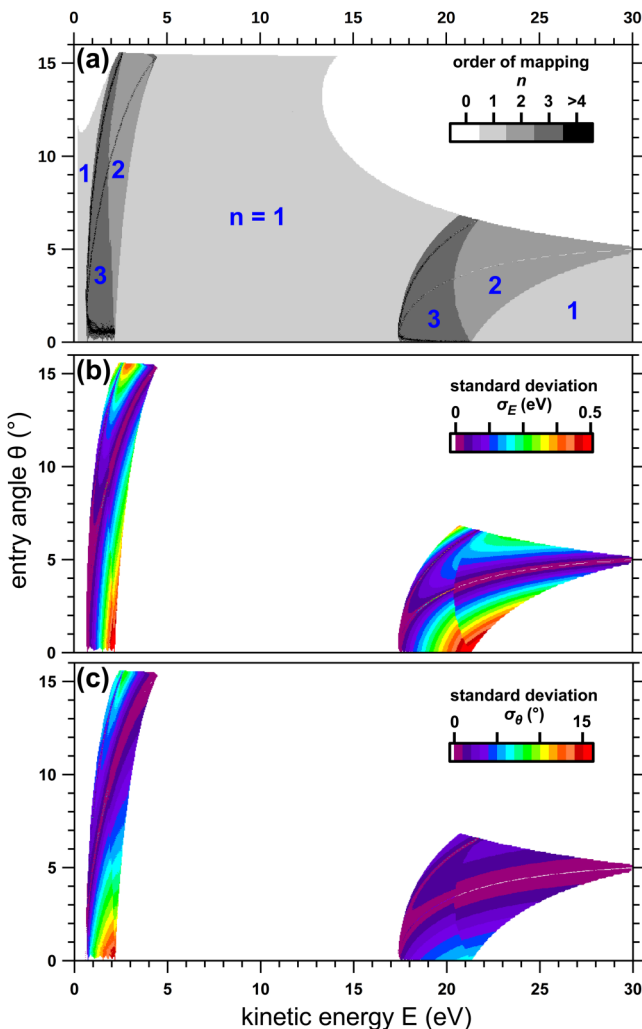


FIG. 4. (a) Order n of the forward mapping,²¹ which transforms events from (θ, E) in Fig. 3(a) to (r, t) in Fig. 3(b). In (b) and (c), the systematic error in energy (σ_E) and angle (σ_θ) according to Eq. (1) due to the approximated backward mapping are shown, respectively. In conventional analysis, only regions with $n = 1$ are considered.

it is homogeneous over the angular and energy range of the many-to-one mapping. For the same spectrometer settings as in Fig. 4(a), the systematic errors σ_E and σ_θ are derived according to Eq. (1) and displayed in Figs. 4(b) and 4(c).

The maximum of the systematic error in energy σ_E for the specific spectrometer settings²¹ in Fig. 4(b) is up to 0.45 eV in the region around 2 eV and around 22 eV for a small range of small emission angles. This value is only about a factor of 2 worse than the energy resolution in the conventional analysis of the spectrometer settings for a wide energy range,²² which may be acceptable for experiments aiming only at a moderate energy resolution. The angular error σ_θ in Fig. 4(c) is smaller than 7° except in the low energy region near $E = 2$ eV or at large entry angles $\theta \geq 14^\circ$. The large σ_θ in these regions can be understood by considering the focus of the ToF spectrometer, where photoelectrons with largely different emission angles are mapped onto a small area near the center $r \approx 0$ of the 2D detector.^{26,27}

For application to other energy ranges, a similar pattern as in Fig. 4(a) needs to be used according to the different kinetic (E_{kin}) and pass energy (E_{pass}) settings of the spectrometer.^{11,21} When increasing E_{kin} , the middle $n = 1$ region in Fig. 4(a) will shift towards higher energies. In addition, the ratio between its energetic extension to the value of E_{pass} will increase as the ratio E_{kin}/E_{pass} increases. As an example, the central $n = 1$ region for $(E_{kin}, E_{pass}) = (8, 60)$ eV has a width of about 15 eV at $\theta = 0^\circ$ as can be seen in Fig. 4(a), and it expands to about 24 eV for the settings of $E_{kin} = 16$ eV at the same E_{pass} . Accordingly, the many-to-one regions on the lower and higher energy sides will be shifted in energy. Moreover, as shown in Fig. 3(a), the many-to-one mapping occurs between (θ, E) coordinates with comparable energies but different angles. Therefore, we may expect that σ_E in Fig. 4(b) would scale with the energy width of the many-to-one regions when varying E_{kin} and E_{pass} , whereas σ_θ could remain sizable as in Fig. 4(c). As shown in Fig. 4(b), the maximum of σ_E for $(E_{kin}, E_{pass}) = (8, 60)$ eV is about 0.45 eV at $E \approx 2$ eV, and it increases up to about 1.3 eV at $E \approx 7$ eV for the settings $(E_{kin}, E_{pass}) = (16, 60)$ eV.

C. Photoelectron spectroscopy (ARPES) on Ag(001)

The approximated backward mapping is demonstrated and compared with conventional one-to-one backward mapping in Fig. 5 for ARPES experiments on a Ag(001) surface. The photoelectrons are excited by a high-order harmonic light source²⁸ and analyzed by the ToF spectrometer presented in Secs. III A and III B. The settings of the spectrometer were a wide-angle-mode with a nominal kinetic energy (E_{kin}) of 8 eV, a pass energy (E_{pass}) of 60 eV. The corresponding energy and angular acceptance ranges are displayed by the grid in Fig. 3(a) as well as by the filled area in Fig. 4(a), having a central one-to-one mapping region within $E = 9 \pm 4$ eV for $\theta = \pm 15^\circ$. The photon flux was estimated as 3×10^5 photons/s, with a pulse duration of around 2 ps, an estimated bandwidth of 70 meV at the 32 eV photon energy, and a spot size measured on the sample of $100 \pm 30 \mu\text{m}$. The total acquisition time was 11 min. In Fig. 5(a), only photoelectron events at the (r, t) detector coordinates with a

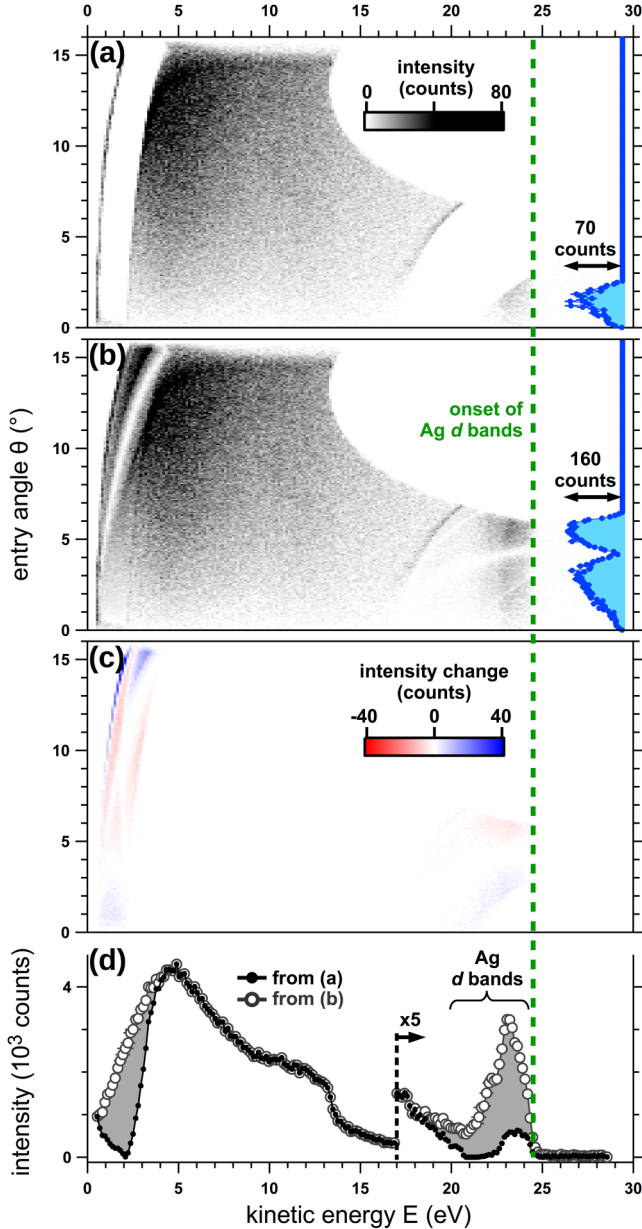


FIG. 5. Distribution of photoelectrons from Ag(001) excited by *s*-polarized light with 32 eV photon energy. Light incidence is parallel to the surface normal, and the entry angle 0° into the spectrometer corresponds to an emission angle of 45° from the surface normal. In (a), only the one-to-one backward mapping is used, and in (b) the approximated backward mapping is additionally applied. In (c), the change in the approximated backward mapping due to a more simplified weighting factor $w_i = 1/n$ is shown. Angle-integrated spectra from (a) and (b) are shown in (d). The dashed line indicates the onset of emission from the Ag *d* bands about 4 eV below the Fermi-level. Filled spectra (blue) in (a) and (b) show the angular distribution integrated from 22 to 24 eV, with an error bar σ_θ in (b) up to 5° according to Fig. 4(c).

one-to-one correspondence to the (θ, E) emission coordinates are considered. In Fig. 5(b), the approximation method in Sec. II is additionally applied on the same measured dataset with the weighting factors in Eq. (2) in order to retrieve events from the *n*-to-one forward mapping by the spectrometer.

By comparing Figs. 5(a) and 5(b), we can clearly see that more photoelectron events are analyzed when the approximated backward mapping is used. More specifically, in the comparison in Fig. 5(d), a fourfold intensity increase

at the Ag *d* bands can be clearly seen when using the approximated backward mapping. Therefore, the approximated backward mapping provides an opportunity to analyze more photoelectron events in an extended energy range as detected by the ToF-spectrometer.

In addition, the angular distributions of Ag *d* electrons from 22 to 24 eV are shown by the filled spectra in Figs. 5(a) and 5(b), with a corresponding error in Fig. 4(c) up to 5° . This sizable error is due to the focusing of electron trajectories with various emission angles near $t = 170$ ns as can be seen in Fig. 3(b). Furthermore, in Fig. 5(c), we show the change in the case of more simplified weighting factors $w_i = 1/n$ instead of Eq. (2). This change may be viewed as an estimation for the systematic error in the intensity.

Last but not least, we discuss the influence of the detector resolution to the spectra in Fig. 5(b). As an example, we consider the energy broadening (ΔE) due to the detector time resolution, which dominates over the contribution of the detector spatial resolution for our settings. From the forward mapping in Sec. III A, we can extract the dependence of the kinetic energy of electron (E) on the time-of-flight (t) as quantified by $(\partial E / \partial t)_r$. This quantity provides an estimation for the energy broadening due to a given resolution of the time-of-flight measurement. With an assumed time resolution $\Delta t \approx 0.24$ ns in the experiments, we estimate an energy resolution by $\Delta t (\partial E / \partial t)_r \approx 180$ meV at around 25 eV. This value is in agreement with our previous experiments with similar settings²² and can be compared with the systematic energy error due to the approximated backward mapping in Fig. 4(b).

IV. SUMMARY

To summarize, we demonstrate an approximation method to extend the energy and angular range of photoelectrons that can be analyzed using time-of-flight (ToF) spectroscopy. Our approximation allows one to analyze photoelectron events whose emission coordinates (θ, ϕ, E) are mapped to the detector coordinates (x, y, t) in a many-to-one mapping. Conventionally, these events are detected in parallel with the events in the one-to-one mapping, but they are abandoned in the data analysis. In the approximation, we assume a given distribution among the multiple emission coordinates (θ_i, ϕ_i, E_i) that correspond to the same (x, y, t) . The resultant systematic errors in the retrieved energy and emission angles have upper bounds, and they are given by the maximum difference between the emission coordinates (θ_i, ϕ_i, E_i) that are mapped to the same detector coordinates (x, y, t) by the spectrometer. As a practical example, we measure photoelectrons from a Ag(001) surface using a commercial ToF spectrometer and analyze them with the approximated backward mapping. As a result, the photoelectrons distributed over a kinetic energy range from 0.5 to 25 eV can be analyzed in parallel. In combination with conventional ToF analysis, our approximation method assists to characterize photoelectrons more efficiently and is important for advanced spectroscopies with demanding statistics, such as coincidence electron spectroscopies at surfaces.^{22,29} In addition, our method may be extended to spectrometers with non-cylindrical symmetries.

ACKNOWLEDGMENTS

Technical support from R. Kulla, F. Helbig, and F. Weiss is gratefully acknowledged. The authors thank Professor J. Kirschner for his long-standing interest and support. This work is partially funded by the Deutsche Forschungsgemeinschaft through SFB-762 (B7, A3) and SFB/TRR-227 (A06).

- ¹N. Mirsaleh-Kohan, W. D. Robertson, and R. N. Compton, *Mass Spectrom. Rev.* **27**, 237 (2008).
- ²A. Benninghoven, *Angew. Chem. Int. Ed.* **33**, 1023 (1994).
- ³G. Schönhense, K. Medjanik, and H.-J. Elmers, *J. Electron. Spectros. Relat. Phenomena* **200**, 94 (2015).
- ⁴D. Kühn, F. Sorgenfrei, E. Giangrisostomi, R. Jay, A. Musazay, R. Ovsyannikov, C. Strählman, S. Svensson, N. Mårtensson, and A. Föhlisch, *J. Electron. Spectros. Relat. Phenomena* **224**, 45 (2018).
- ⁵K. Medjanik, O. Fedchenko, S. Chernov, D. Kutnyakhov, M. Ellguth, A. Oelsner, B. Schönhense, T. R. F. Peixoto, P. Lutz, C.-H. Min, F. Reinert, S. Däster, Y. Acremann, J. Viehhaus, W. Wurth, H. J. Elmers, and G. Schönhense, *Nat. Mater.* **16**, 615–621 (2017).
- ⁶C. Tusche, P. Goslawski, D. Kutnyakhov, M. Ellguth, K. Medjanik, H. J. Elmers, S. Chernov, R. Wallauer, D. Engel, A. Jankowiak, and G. Schönhense, *Appl. Phys. Lett.* **108**, 261602 (2016).
- ⁷D. Kutnyakhov, S. Chernov, K. Medjanik, R. Wallauer, C. Tusche, M. Ellguth, S. A. Nepijko, M. Krivenkov, J. Braun, S. Borek, J. Minár, H. Ebert, H. J. Elmers, and G. Schönhense, *Sci. Rep.* **6**, 29394 (2016).
- ⁸U. B. Cappel, S. Plogmaker, J. A. Terschlüsen, T. Leitner, E. M. J. Johansson, T. Edvinsson, A. Sandell, O. Karis, H. Siegbahn, S. Svensson, N. Mårtensson, H. Rensmo, and J. Söderström, *Phys. Chem. Chem. Phys.* **18**, 21921 (2016).
- ⁹C. Strählman, R. Sankari, M. Lundqvist, G. Öhrwall, R. Ovsyannikov, S. Svensson, N. Mårtensson, and R. Nyholm, *J. Phys. Conf. Ser.* **425**, 092011 (2013).
- ¹⁰P. D. C. King, R. C. Hatch, M. Bianchi, R. Ovsyannikov, C. Lupulescu, G. Landolt, B. Slomski, J. H. Dil, D. Guan, J. L. Mi, E. D. L. Rienks, J. Fink, A. Lindblad, S. Svensson, S. Bao, G. Balakrishnan, B. B. Iversen, J. Osterwalder, W. Eberhardt, F. Baumberger, and P. Hofmann, *Phys. Rev. Lett.* **107**, 096802 (2011).
- ¹¹M. H. Berntsen, O. Götzberg, and O. Tjernberg, *Rev. Sci. Instrum.* **82**, 095113 (2011).
- ¹²A. Oelsner, O. Schmidt, M. Schicketanz, M. Klais, G. Schönhense, V. Mergel, O. Jagutzki, and H. Schmidt-Boecking, *Rev. Sci. Instrum.* **72**, 3968 (2001).
- ¹³R. Ovsyannikov, P. Karlsson, M. Lundqvist, C. Lupulescu, W. Eberhardt, A. Föhlisch, S. Svensson, and N. Mårtensson, *J. Electron Spectros. Relat. Phenomena* **191**, 92 (2013).
- ¹⁴B. Wannberg, *Nuclear Instrum. Methods Phys. Res. A* **601**, 182 (2009).
- ¹⁵A. Trützscher, M. Huth, C.-T. Chiang, R. Kamra, F. O. Schumann, J. Kirschner, and W. Widdra, *Phys. Rev. Lett.* **118**, 136401 (2017).
- ¹⁶T. Arion and U. Hergenbühler, *J. Electron Spectros. Relat. Phenomena* **200**, 222 (2015).
- ¹⁷F. O. Schumann, C. Winkler, and J. Kirschner, *Phys. Status Solidi (b)* **246**, 1483 (2009).
- ¹⁸G. Stefani, S. Iacobucci, A. Ruocco, and R. Gotter, *J. Electron Spectrosc. Relat. Phenom.* **127**, 1 (2002).
- ¹⁹M. Hattass, T. Jahnke, S. Schössler, A. Czausch, M. Schöffler, L. P. H. Schmidt, B. Ulrich, O. Jagutzki, F. O. Schumann, C. Winkler, J. Kirschner, R. Dörner, and H. Schmidt-Böcking, *Phys. Rev. B* **77**, 165432 (2008).
- ²⁰This simplified argument is valid for cases where the angular acceptance does not strongly depend on the energy, and it can be refined by considering the energy dependent joint acceptance.
- ²¹Themis 1000, SPECS Surface Nano Analysis GmbH, Berlin, Germany.
- ²²M. Huth, C.-T. Chiang, A. Trützscher, F. O. Schumann, J. Kirschner, and W. Widdra, *Appl. Phys. Lett.* **104**, 061602 (2014).
- ²³ σ_E^{max} occurs when, for example, $w_1 = 1$, $w_2 = 0$, $E_1 = E_{max}$, and $E_{in} = E_2 = E_{min}$.
- ²⁴The spectrometer model is provided by the manufacturer,²¹ and the trajectories of photoelectrons are calculated by the commercial program: SIMION, version 8, Scientific Instrument Services, Inc., USA.
- ²⁵In experiments, the position of $r = 0$ can be estimated by the focusing of electron trajectories with various emission angles θ at a given time-of-flight t , for example, near $t = 170$ ns in Fig. 3(b).
- ²⁶T. Mulvey and M. J. Wallington, *Rep. Prog. Phys.* **36**, 347 (1973).
- ²⁷A. B. El-Kareh and J. C. J. El-Kareh, *Electron Beams, Lenses, and Optics* (Academic Press, 1970), pp. 185–245.
- ²⁸C.-T. Chiang, M. Huth, A. Trützscher, F. O. Schumann, J. Kirschner, and W. Widdra, *J. Electron Spectros. Relat. Phenomena* **200**, 15 (2015).
- ²⁹C. Lupulescu, T. Arion, U. Hergenbühler, R. Ovsyannikov, M. Förstel, G. Gavrila, and W. Eberhardt, *J. Electron Spectros. Relat. Phenomena* **191**, 104 (2013).